Catalysis Communications 62 (2015) 29–33

Contents lists available at ScienceDirect

Catalysis Communications

journal homepage: www.elsevier.com/locate/catcom

Short communication

Synthesis and characterization of $S_2O_8^{2-}/ZnFe_xAl_{2-x}O_4$ solid acid catalysts for the esterification of acetic acid with *n*-butanol

Junxia Wang [a,*], Hui Pan [a,b], Anqi Wang [a], Xiaoyun Tian [a], Xiuling Wu [a], Yongqian Wang [a]

[a] Faculty of Materials Science and Chemistry, Engineering Research Center of Nano-Geomaterials of Ministry of Education, China University of Geosciences, Wuhan 430074, China
[b] College of Chemistry and Chemical Engineering, Xinjiang Normal University, Urumqi 830054, China

ARTICLE INFO

Article history:
Received 10 November 2014
Received in revised form 5 January 2015
Accepted 6 January 2015
Available online 8 January 2015

Keywords:
Solid acid
$S_2O_8^{2-}/ZnFe_xAl_{2-x}O_4$
Synthesis
Characterization
Catalytic properties

ABSTRACT

New spinel-types of $S_2O_8^{2-}/ZnFe_xAl_{2-x}O_4$ solid acid catalysts were prepared by sol–gel method. Their catalytic performances for the synthesis of *n*-butyl acetate were investigated. The catalysts were characterized by means of XRD, IR, XPS, FT-IR of adsorbed pyridine and NH_3-TPD. The experimental results showed that $S_2O_8^{2-}/ZnFe_xAl_{2-x}O_4$ solid acid catalysts maintained the spinel structure as well as the support of $ZnFe_xAl_{2-x}O_4$. Fe^{3+} ions were well incorporated and highly dispersed into the spinel lattice. $S_2O_8^{2-}/ZnFe_{0.15}Al_{1.85}O_4$ exhibited the maximum conversion of acetic acid with 98.2%. Moreover, $S_2O_8^{2-}/ZnFe_{0.15}Al_{1.85}O_4$ showed better reusability, which remained above 72.7% conversion of acetic acid even after being used five times.

1. Introduction

SO_4^{2-}/M_xO_y solid acid catalysts have received extensive interests in recent years because of their strong acidity, high catalytic activity, easy separation, low waste generation, good environmental friendliness, etc. [1,2]. Among them, SO_4^{2-}/ZrO_2, SO_4^{2-}/SnO_2 and SO_4^{2-}/TiO_2 have drawn significant attention due to their good catalytic performances in many reactions [3–5]. However, they have similar disadvantages of rapid deactivation and low service life, which limit their practical application [6]. The modification by the addition of other metal ions is usually considered as an effective method to overcome their limitation. However, the crystal type is easily changed and difficult to control in the process of doping with other metal ions, which has a great influence on the formation of acid sites and catalytic performances of SO_4^{2-}/M_xO_y. For instance the monochromic in ZrO_2 and SnO_2 crystallization is not conducive to the formation of acid centers. By comparison, the classical tetragonal phase is beneficial to improve the acid catalytic activity of SO_4^{2-}/ZrO_2 and SO_4^{2-}/SnO_2 [7–9]. TiO_2 has three main forms of crystal, including the anatase, rutile, and brookite. Among them, the anatase is conducive to improve the catalytic performance of SO_4^{2-}/TiO_2 [10]. In order to control the crystal transformation, scholars have performed much research [10,11]. Nevertheless, the factors that influence the crystal form of simple oxides are complex and difficult to control. Therefore, researchers in this field are focusing on looking for a new type of support.

Spinel compound oxides have the advantage of stable structure, single crystal shape and easy modification, which can generally be described by the chemical formula of AB_2O_4 [12–15]. Recently, some scholars found that spinel compound oxides could be used in the synthesis of SO_4^{2-}/M_xO_y solid acid. For example, Lin et al. reported that $SO_4^{2-}/CoFe_2O_4$ solid acid displayed certain acid strength and good catalytic activity in the synthesis of ethyl acetate reaction [16]. Lee et al. found that sulfated $ZnFe_2O_4$ showed a better catalytic performance in the oxidative dehydrogenation of *n*-butene because of its good acidity [17]. Nanosized $SO_4^{2-}/ZnFe_2O_4$ catalyst was found to be highly active in some important acid catalyzed reactions [18]. From the literature mentioned above, it could be seen that spinel oxides could be used as a new support for the preparation of solid acid catalyst. Nevertheless, there is still little information about this aspect of research in the literature.

In this paper, new spinel-types of $S_2O_8^{2-}/ZnFe_xAl_{2-x}O_4$ solid acid catalysts were prepared and applied in the synthesis of *n*-butyl acetate. The effects of *x* value on the catalytic activities of $S_2O_8^{2-}/ZnFe_xAl_{2-x}O_4$ were studied. In addition, the structure, the acidity, and the stability of $S_2O_8^{2-}/ZnFe_xAl_{2-x}O_4$ were evaluated. At present, little attention has been paid to the study of $S_2O_8^{2-}/ZnFe_xAl_{2-x}O_4$ solid acid catalyst. This study was aimed to provide some valuable information on the application of $S_2O_8^{2-}/ZnFe_xAl_{2-x}O_4$ in the esterification reaction.

* Corresponding author.
E-mail address: jxwyqh@sina.com (J. Wang).

http://dx.doi.org/10.1016/j.catcom.2015.01.009
1566-7367/

2. Experimental

2.1. Catalyst preparation

Spinel $ZnFe_xAl_{2-x}O_4$ ($x = 0, 0.1, 0.15, 0.2$) were prepared as follows: $Al(NO_3)_3 \cdot 9H_2O$, $Zn(NO_3)_3 \cdot 6H_2O$ and $Fe(NO)_3 \cdot 9H_2O$ were dissolved in alcohol. 5 wt.% of polyethylene glycol was then slowly added to the solution under magnetic stirring at room temperature for 4 h. The obtained mixture was further stirred for 2 h in a water bath at 60 °C. After the mixture was dried at 120 °C, the precursor was obtained. After being ground into a fine powder, the obtained powder was calcined at 600 °C for 5 h in air sequentially to obtain the powder samples. The obtained spinel compound oxides were designated as $ZnFe_xAl_{2-x}O_4$, where x represented the different molar ratios of Fe (based on the compositions of $ZnAl_2O_4$). $S_2O_8^{2-}/ZnFe_xAl_{2-x}O_4$ catalysts were prepared by impregnating calcined $ZnFe_xAl_{2-x}O_4$ sample using 1.50 mol/L aqueous ammonium persulfate ($(NH_4)_2S_2O_8$) solution. Sulfation was done by immersing 1 g of $ZnFe_xAl_{2-x}O_4$ in 10 mL of ammonium persulfate solution for 12 h. After been filtered and dried, the obtained samples were calcined at 550 °C for 5 h to get $S_2O_8^{2-}/ZnFe_xAl_{2-x}O_4$.

2.2. Catalyst characterization

XRD measurements were performed on a Dmax-3β diffractometer. IR spectra of the catalysts were recorded by a Nicolet 6700 spectrometer using KBr pellets. FT-IR of adsorbed pyridine spectra were recorded on a Frontier FT-IR spectrometer. Before measurement, the sample was pretreated at 300 °C for 1 h in a vacuum. Then the samples were cooled to 30 °C and adsorbed pyridine vapor for 0.5 h. The adsorbed pyridine was subsequently removed by degassing for 1 h at 150 °C. Then, the FT-IR spectra of the adsorbed pyridine were recorded. The X-ray photoelectron spectroscopy (XPS) was performed in a VG Multilab 2000. The NH_3 temperature programmed desorption (NH_3-TPD) experiments were carried out using a Micromeritics AutoChem II 2920 quipped with a TCD detector. The samples were treated in helium flow (50 mL/min) at 400 °C for 1 h and exposed to NH_3 (50 mL/min) at room temperature for 1 h, and then followed by helium to remove gas-phase and physically adsorbed NH_3. Measurements were started in helium with a heating rate of 10 °C/min.

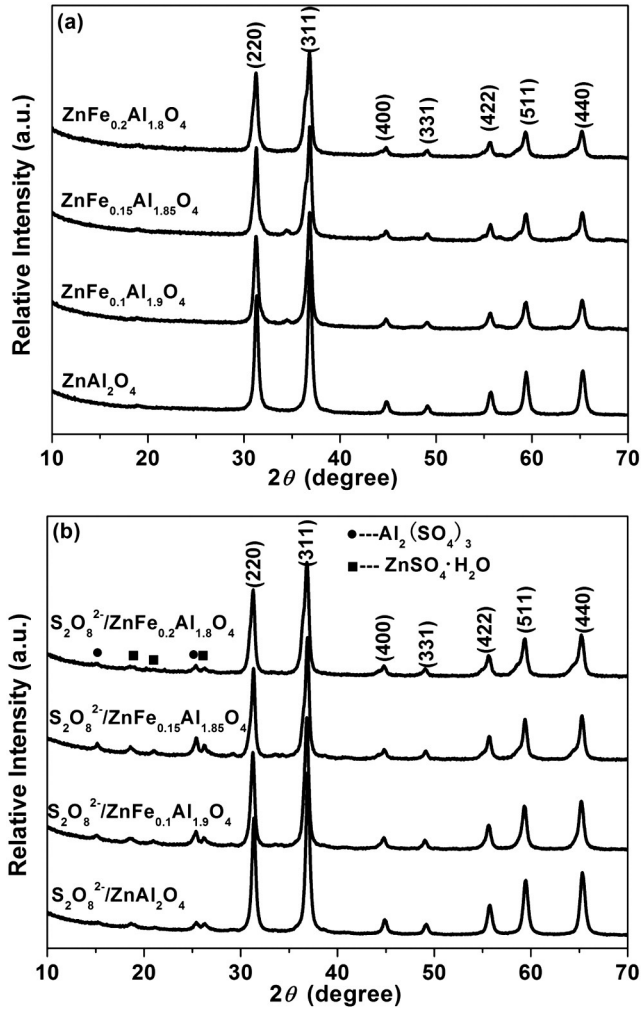

Fig. 1. XRD patterns of $ZnFe_xAl_{2-x}O_4$ (a) and $S_2O_8^{2-}/ZnFe_xAl_{2-x}O_4$ (b).

2.3. Catalytic activity test

The esterification reaction was carried out in a three-necked flask under atmospheric pressure, which is equipped with a magnetic stirrer, a thermometer and a refluxing condenser tube. The reaction conditions were as follows: the reaction temperatures were 115–118 °C, the molar ratio of *n*-butanol to acetic acid was 3:1, the reaction time was 3 h and the catalyst amount was 1.55 wt.% (weight percentage of the reaction mixture). After the reaction, the catalyst was immediately separated from the reaction mixture by filtering. Then, the titration experiment was rapidly performed, which was used to determine the residual acid. Namely, 0.50 mL reaction mixture was added in 20.00 mL absolute alcohol and titrated by 0.10 mol/L NaOH solution using phenolphthalein as an indicator. Then, the conversion of acetic acid was measured using the following equation [19,20]:

$$\text{The conversion of acetic acid}(\%) = \frac{M_0 - M_1}{M_0} \times 100$$

where M_0 was the dissipative volume of NaOH solution before reaction and M_1 was the dissipative volume of NaOH solution after reaction.

In order to test the stability, $S_2O_8^{2-}/ZnAl_2O_4$ and $S_2O_8^{2-}/ZnFe_{0.15}Al_{1.85}O_4$ were repeatedly used for the batch reaction process. After each catalytic evaluation was finished, the catalyst was filtered from the reaction mixture, and dried at 60 °C for 12 h in air. Then, the catalyst without any further intermediate reactivation was reused in a new reaction cycle under the same reaction conditions.

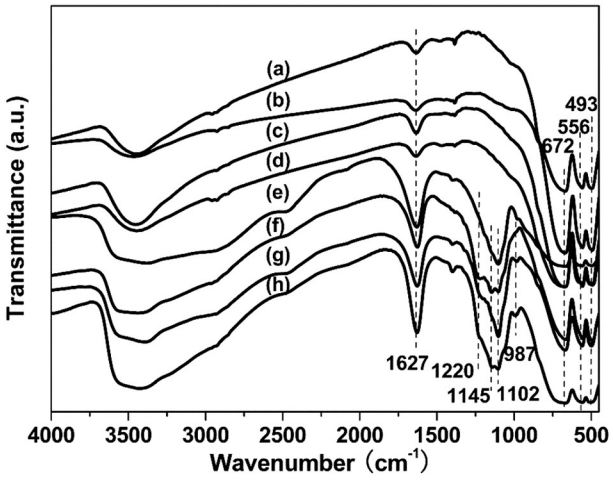

Fig. 2. IR spectra of $ZnFe_xAl_{2-x}O_4$ and $S_2O_8^{2-}/ZnFe_xAl_{2-x}O_4$. (a) $ZnFe_{0.2}Al_{1.8}O_4$, (b) $ZnFe_{0.15}Al_{1.85}O_4$, (c) $ZnFe_{0.1}Al_{1.9}O_4$, (d) $ZnAl_2O_4$, (e) $S_2O_8^{2-}/ZnAl_2O_4$, (f) $S_2O_8^{2-}/ZnFe_{0.1}Al_{1.9}O_4$, (g) $S_2O_8^{2-}/ZnFe_{0.15}Al_{1.85}O_4$, and (h) $S_2O_8^{2-}/ZnFe_{0.2}Al_{1.8}O_4$.

3. Results and discussion

3.1. Catalyst characterization

The XRD patterns of $ZnFe_xAl_{2-x}O_4$ and $S_2O_8^{2-}/ZnFe_xAl_{2-x}O_4$ are present in Fig. 1. As shown in Fig. 1(a), all the reflection peaks of $ZnFe_xAl_{2-x}O_4$ match well with the standard JCPDS card No. 82-1043 of spinel $ZnAl_2O_4$, indicating that all the samples of $ZnFe_xAl_{2-x}O_4$ crystallize single spinel structure. Furthermore, there are no apparent changes in the intensity and the position of the characteristic peaks with the *x*-value increase, indicating that Fe^{3+} ions are well incorporated and highly dispersed into the spinel lattice. As shown in Fig. 1(b), $S_2O_8^{2-}/ZnFe_xAl_{2-x}O_4$ maintained the spinel structure as well as the support of $ZnFe_xAl_{2-x}O_4$. However, $Al_2(SO_4)_3$ and $ZnSO_4 \cdot H_2O$ crystalline phases are observed in all samples of $S_2O_8^{2-}/ZnFe_xAl_{2-x}O_4$, which might be attributed to the interaction between excess $S_2O_8^{2-}$ and metal ions. A similar phenomenon is observed in other SO_4^{2-}/M_xO_y solid acid [21].

The IR spectra of $ZnFe_xAl_{2-x}O_4$ and $S_2O_8^{2-}/ZnFe_xAl_{2-x}O_4$ are shown in Fig. 2. Bands at 672 cm^{-1}, 556 cm^{-1} and 493 cm^{-1} are related to Al – O stretching vibrations, Zn – O stretching vibrations and Al – O bending vibrations respectively [22,23]. In addition, spectra of the $S_2O_8^{2-}/ZnFe_xAl_{2-x}O_4$ exhibit the special bands in the range of 900–1400 cm^{-1}, which are associated with the acid structures of the catalysts [24–26]. The specific bands in this region are attributed to the strong interaction between sulfuric groups and metal ions, which are correlated to their high catalytic activities. Among them, the bands at 987 cm^{-1}, 1102 cm^{-1} and 1145 cm^{-1} are assigned to the stretching vibration of S – O. In the meantime, the band at 1220 cm^{-1} is assigned to the stretching vibration of S═O, indicating that $S_2O_8^{2-}$ ion coordinates to metal ions and forms the bidentate structure [25]. Such a bidentate structure is believed to be a driving force in the generation of many acidic sites on surface of sulfated metal oxides, making the samples possess acidity. Noticeably, the typical bands in the range of 900–1400 cm^{-1} are not observed in the case of $ZnFe_xAl_{2-x}O_4$. However, upon impregnation with

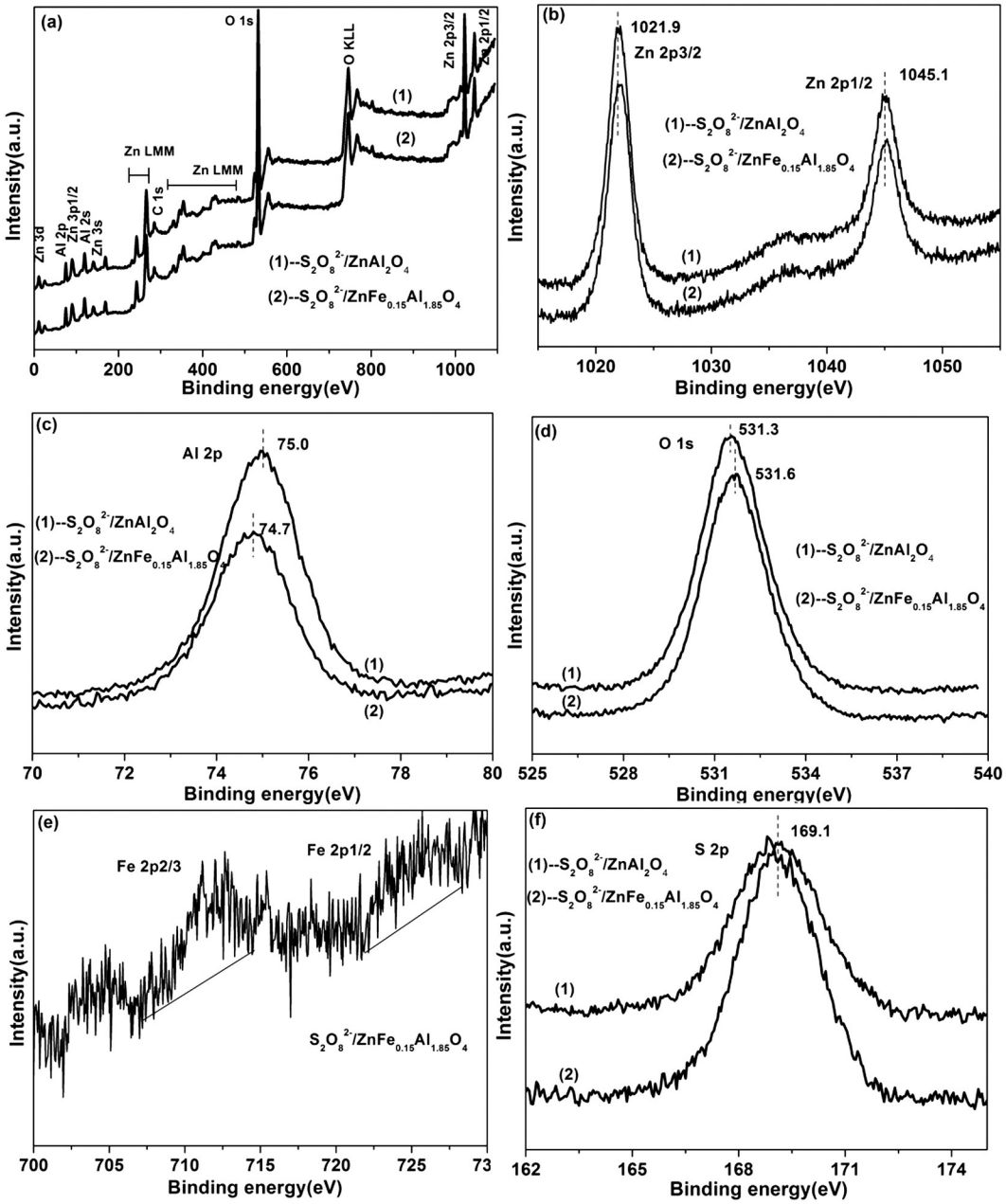

Fig. 3. XPS spectra of $S_2O_8^{2-}/ZnAl_2O_4$ and $S_2O_8^{2-}/ZnFe_{0.15}Al_{1.85}O_4$. (a) The whole XPS spectra, (b) Zn 2p spectra, (c) Al 2p spectra, (d) O 1s spectra, (e) Fe 2p spectra, and (f) S 2p spectra.

ammonium persulfate, there is a drastic change in the IR spectra of the samples. All related bands in the range of 900–1400 cm^{-1} become obvious in $S_2O_8^{2-}/ZnFe_xAl_{2-x}O_4$ samples. This result indicates a very strong interaction of surface sulfate species with metal ions, which is the significant reason for the formation of the active acid center on the surface of $S_2O_8^{2-}/ZnFe_xAl_{2-x}O_4$. The similar conclusion was also proved by other SO_4^{2-}/M_xO_y systems [27].

The XPS analysis of $S_2O_8^{2-}/ZnAl_2O_4$ and $S_2O_8^{2-}/ZnFe_{0.15}Al_{1.85}O_4$ is shown in Fig. 3. For $S_2O_8^{2-}/ZnAl_2O_4$, the Zn $2p_{3/2}$ and Zn $2p_{1/2}$ binding energies are located at 1021.9 eV and 1045.1 eV, respectively, which are close to the standard data for Zn^{2+} (Fig. 3(b)) [28]. The peaks located at 75.0 eV and 531.3 eV are attributed to the Al 2p (Fig. 3(c)) and O 1s (Fig. 3(d)) binding energies, respectively [29,30]. Compared with $S_2O_8^{2-}/ZnAl_2O_4$, the XPS spectra of $S_2O_8^{2-}/ZnFe_{0.15}Al_{1.85}O_4$ sample show no significant differences in the binding energies of the Zn $2p_{3/2}$ and Zn $2p_{1/2}$. However, the Al 2p shifts to the lower binding energy and the O 1s shifts to the higher binding energy. From the above result, we speculate that the introduction of iron instead of aluminum in the spinel lattice could change the chemical environment of the measured atoms in the crystal lattice, which may be a reason for the influence of the acid properties and catalytic activities. The peaks at 711.5 and 725.8 eV are corresponding to the Fe $2p_{3/2}$ and Fe $2p_{1/2}$ for Fe^{3+} respectively (Fig. 3(e)) [31]. In the meantime, the peak at 169.1 eV is measured for S 2p binding energy in the two samples (Fig. 3(f)), which is attributable to the sulfur oxidation state of +6. Specifically, the sulfur oxidation state of +6 plays a key role on the formation of the strong acidity [32]. This result is in good agreement with the IR results.

Table 1
The effect of x value on the catalytic activities of $S_2O_8^{2-}/ZnFe_xAl_{2-x}O_4$ solid acids.

Catalysts	The conversion of acetic acid (%)
No	38.8%
$ZnFe_{0.15}Al_{1.85}O_4$	47.5%
$S_2O_8^{2-}/ZnAl_2O_4$	91.4%
$S_2O_8^{2-}/ZnFe_{0.1}Al_{1.9}O_4$	95.2%
$S_2O_8^{2-}/ZnFe_{0.15}Al_{1.85}O_4$	98.2%
$S_2O_8^{2-}/ZnFe_{0.2}Al_{1.8}O_4$	92.5%

FT-IR spectra of adsorbed pyridine made it possible to distinguish between Brönsted and Lewis acid sites. As shown in Fig. 4(a), the peak at 1540 cm^{-1} is attributable to Brönsted acid sites. The peak at 1450 cm^{-1} is assigned to Lewis acid sites [33,34]. The band at 1490 cm^{-1} is attributed to both Brönsted and Lewis acid sites. FT-IR spectra of the adsorbed pyridine therefore indicate that both Brönsted and Lewis acid sites are present on the surface of $S_2O_8^{2-}/ZnFe_xAl_{2-x}O_4$. Obviously, the concentration of Brönsted and Lewis acid sites of $S_2O_8^{2-}/ZnAl_2O_4$ is the lowest among all samples. Meanwhile, $S_2O_8^{2-}/ZnFe_{0.15}Al_{1.85}O_4$ has the larger number of acid sites, resulting in its highest catalytic activities. This result is also confirmed by the NH_3-TPD results.

The acid strength distribution obtained from the NH_3-TPD spectra of $ZnFe_{0.15}Al_{1.85}O_4$ and $S_2O_8^{2-}/ZnFe_xAl_{2-x}O_4$ is shown in Fig. 4(b). The peaks in each of the profiles correspond to desorption of NH_3 bound to the acid sites of oxide surface. The desorption temperature indicates the acid strength of the catalyst. Generally, NH_3 adsorbed on the weak acid sites is desorbed at low temperature. Correspondingly, NH_3 adsorbed on strong acid sites is desorbed at high temperature. The higher temperature of desorption is, the stronger the acid strength is. As shown in Fig. 4(b), $ZnFe_{0.15}Al_{1.85}O_4$ exhibits almost no desorption peaks in the range of 100 °C and 800 °C, which could be one reason for its lower catalytic activity (as shown in Table 1). However, $S_2O_8^{2-}/ZnFe_xAl_{2-x}O_4$ all show broad desorption peaks in the range of 100 °C and 800 °C, indicating that $S_2O_8^{2-}$ ion coordinates to metal ions and forms the acid structures. The NH_3-TPD results are consistent very well with the IR results. The peaks below 450 °C are corresponding to the weak and middle strength acid sites. The peaks between 450 °C and 650 °C are attributable to strong acidic sites. The peaks above 700 °C are associated with very strong acidic sites. Compared with $S_2O_8^{2-}/ZnAl_2O_4$, $S_2O_8^{2-}/ZnFe_xAl_{2-x}O_4$ ($x = 0.1, 0.15, 0.2$) shows the stronger acid strength and a greater number of acid sites. It demonstrates that the appropriate addition of Fe results in increasing the amount of acid sites and strengthening the acidity. This result indicates that a certain addition of Fe plays a prior effect on the interaction of the active sulfur

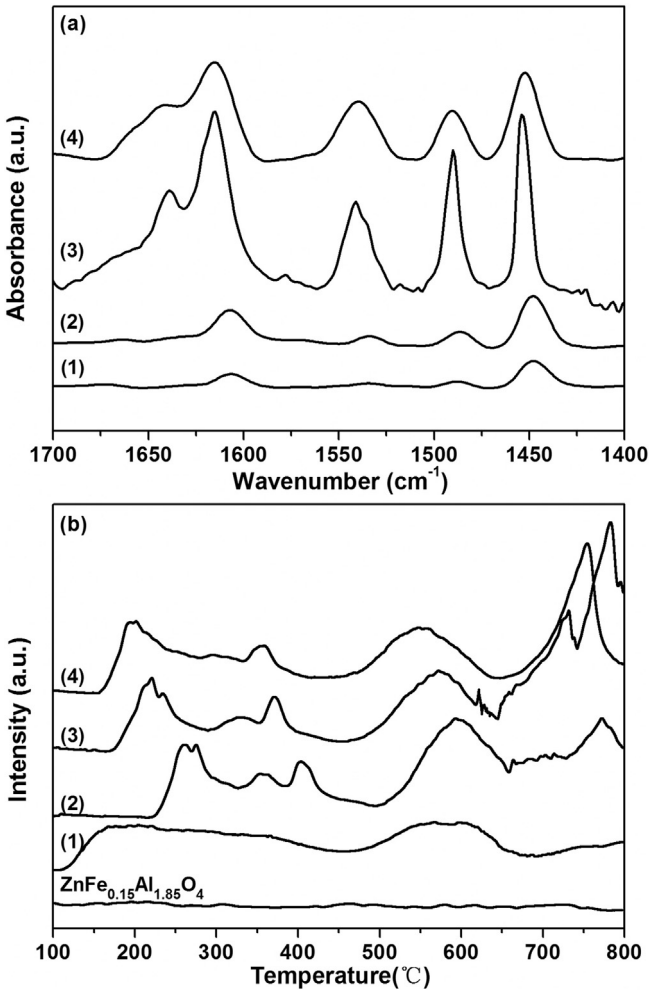

Fig. 4. The pyridine adsorption FT-IR spectra of $S_2O_8^{2-}/ZnFe_xAl_{2-x}O_4$ (a) and NH_3-TPD spectra of $ZnFe_{0.15}Al_{1.85}O_4$ and $S_2O_8^{2-}/ZnFe_xAl_{2-x}O_4$ (b). (1) $S_2O_8^{2-}/ZnAl_2O_4$, (2) $S_2O_8^{2-}/ZnFe_{0.2}Al_{1.8}O_4$, (3) $S_2O_8^{2-}/ZnFe_{0.15}Al_{1.85}O_4$, and (4) $S_2O_8^{2-}/ZnFe_{0.1}Al_{1.9}O_4$.

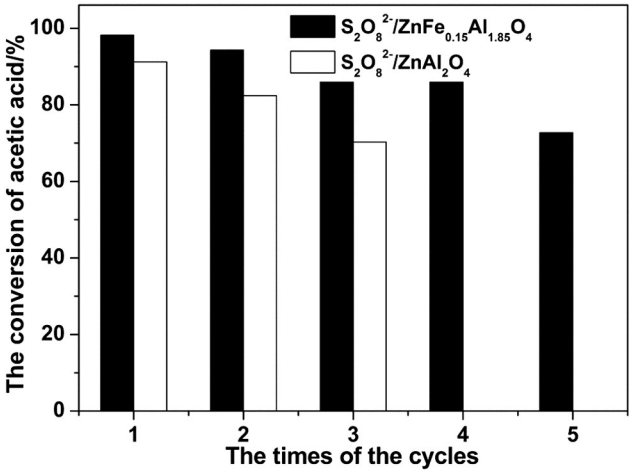

Fig. 5. The reusability of $S_2O_8^{2-}/ZnAl_2O_4$ and $S_2O_8^{2-}/ZnFe_{0.15}Al_{1.85}O_4$.

species with metal oxides. Furthermore, the total acid sites of $S_2O_8^{2-}/ZnFe_{0.15}Al_{1.85}O_4$ are the maximum in all samples, which is consistent with the FT-IR of adsorbed pyridine. Accordingly, $S_2O_8^{2-}/ZnFe_{0.15}Al_{1.85}O_4$ shows the highest activity in all samples.

3.2. Catalytic activities and reusability

Table 1 gives the effect of x value on the catalytic activity of $S_2O_8^{2-}/ZnFe_xAl_{2-x}O_4$ in esterification of acetic acid with *n*-butanol. For comparison, the catalytic activities of $ZnFe_{0.15}Al_{1.85}O_4$ and no catalyst are also added in Table 1. It is found that the conversion of acetic acid is less than 40% in the absence of catalyst. Additionally, the support of $ZnFe_{0.15}Al_{1.85}O_4$ also shows lower catalytic activity with 47.5% conversion of acetic acid. However, $S_2O_8^{2-}/ZnFe_xAl_{2-x}O_4$ catalysts all exhibit significantly high catalytic activities with above 90% conversion of acetic acid. It is well known that acid property of metal oxides is promoted by the surface modification with sulfate ion. According to the IR results, $S_2O_8^{2-}/ZnFe_xAl_{2-x}O_4$ catalysts exhibit the apparent acid structures, indicating that there are strong interactions between sulfuric groups and metal ions. So, the enhanced acidities of sulfated $ZnFe_xAl_{2-x}O_4$ catalysts may be responsible for their higher catalytic activities. By comparison of $S_2O_8^{2-}/ZnAl_2O_4$, $S_2O_8^{2-}/ZnFe_xAl_{2-x}O_4$ ($x = 0.1$–0.2) catalysts present better catalytic activities, which is well associated with their more amount of acid sites. Combined with the characterization results, we could deduce that there might be two main reasons for this phenomenon. First reason is that Fe^{3+} ions instead of Al^{3+} in the spinel lattice change the chemical state of the exterior atom and enhance the acidities of $S_2O_8^{2-}/ZnFe_xAl_{2-x}O_4$. Second, the mixture of different metal ions also modifies acid sites and indirectly helps to improve the catalytic activities [35]. Furthermore, $S_2O_8^{2-}/ZnFe_{0.15}Al_{1.85}O_4$ exhibits the highest catalytic activity with 98.2% conversion of acetic acid. Based on the results of FT-IR of adsorbed pyridine and NH_3-TPD, this result may be owing to its strongest acid strength and its maximum amount of acid sites in all samples.

It is well known that SO_4^{2-}/M_xO_y solid acid catalysts suffer from poor reusability and ongoing deactivation, which is mainly due to the loss of sulfur species as well as carbon deposition [6]. However, there is little recycling data about SO_4^{2-}/M_xO_y solid acid catalysts in the literature, which is vital in the evaluation of a catalyst lifetime. Therefore, $S_2O_8^{2-}/ZnAl_2O_4$ and $S_2O_8^{2-}/ZnFe_{0.15}Al_{1.85}O_4$ solid acid catalysts were recycled to study their stability under use. The results are shown in Fig. 5. Compared with $S_2O_8^{2-}/ZnAl_2O_4$, $S_2O_8^{2-}/ZnFe_{0.15}Al_{1.85}O_4$ shows better reusability, which remains above 72.7% conversion of acetic acid even after being used five times. This above result indicates that the addition of Fe can also enhance the stability of $S_2O_8^{2-}/ZnFe_xAl_{2-x}O_4$ solid acid catalyst.

4. Conclusions

All the samples of $ZnFe_xAl_{2-x}O_4$ and $S_2O_8^{2-}/ZnFe_xAl_{2-x}O_4$ belonged to the stable and unique spinel structure. The introduction of Fe in the crystal lattice of spinel changed the chemical environment of the atoms, which led to an increase of the acid strength and the acid site number. Correspondingly, $S_2O_8^{2-}/ZnFe_xAl_{2-x}O_4$ ($x = 0.1$, 0.15, 0.2) solid acid catalysts showed the higher catalytic activity than $S_2O_8^{2-}/ZnAl_2O_4$ catalyst for the esterification of *n*-butanol with acetic acid. Among them, $S_2O_8^{2-}/ZnFe_{0.15}Al_{1.85}O_4$ showed the highest activity and improved reusability, which has potential applications for other acid catalyzed reactions, either Brönsted acid or Lewis acid.

Acknowledgments

The authors gratefully acknowledge the financial support from NSFC (21203170, 41172051), SFBSRCC (CUGL090227), ERCNGME (CUGNGM 20133), Self-DIRFC (2013-09) and NCSITP (201310491019).

References

[1] S.D. Salim, K.G. Akamanchi, Catal. Commun. 12 (2011) 1153–1156.
[2] D.C. Boffito, V. Crocellà, C. Pirola, B. Neppolian, G. Cerrato, M. Ashokkumar, C.L. Bianchi, J. Catal. 297 (2013) 17–26.
[3] V.G. Devulapelli, H.S. Weng, Catal. Commun. 10 (2009) 1711–1717.
[4] F.H. Alhassan, U. Rashid, M.S. Al-Qubaisi, A. Rasedee, Y.H. Taufiq-Yap, Powder Technol. 253 (2014) 809–813.
[5] M.K. Lam, K.T. Lee, A.R. Mohamed, Appl. Catal. B 93 (2009) 134–139.
[6] X.J. Shi, Y.L. Wua, P.P. Li, H.F. Yi, M.D. Yang, G.H. Wang, Carbohydr. Res. 346 (2011) 480–487.
[7] F. Ye, Z.W. Dong, H.J. Zhang, Catal. Commun. 10 (2009) 2056–2059.
[8] B.M. Reddy, G.K. Reddy, K.N. Rao, L. Katta, J. Mol. Catal. A 306 (2009) 62–68.
[9] C.H. Li, Y.X. Zhao, B. Dai, J. Ind. Eng. Chem. 18 (2012) 520–525.
[10] J.R. Sohn, D.C. Shin, Appl. Catal. B 77 (2008) 386–394.
[11] N. Thimmaraju, S.Z. Mohamed Shamshuddin, S.R. Pratap Venkatesh, J. Mol. Catal. A 391 (2014) 55–65.
[12] G.L. Fan, J. Wang, F. Li, Catal. Commun. 15 (2011) 113–117.
[13] R.T. Kumar, N.C.S. Selvam, C. Ragupathi, L.J. Kennedy, J.J. Vijaya, Powder Technol. 224 (2012) 147–154.
[14] F. Davar, M. Salavati-Niasari, J. Alloys Compd. 509 (2011) 2487–2492.
[15] A. Ghasemin, M. Mousavinia, Ceram. Int. l40 (2014) 2825–2834.
[16] D.J. Lin, S.F. Shen, H.B. Pan, N.S. Chen, Chin. J. Inorg. Chem. 16 (2000) 757–762.
[17] H. Lee, J.C. Jung, I.K. Song, Catal. Lett. 133 (2009) 321–327.
[18] S.V. Jadhav, K.M. Jinka, H.C. Bajaj, Catal. Today 198 (2012) 98–105.
[19] S. Praserthdam, B. Jongsomjit, Catal. Lett. 130 (2009) 583–587.
[20] H.Q. Yang, H.Y. Song, H. Zhang, P. Chen, Z.X. Zhao, J. Mol. Catal. A 381 (2014) 54–60.
[21] R.P. Yao, M.J. Zhang, J. Yang, D.L. Yi, J. Xu, F. Deng, Y. Yue, C.H. Ye, Acta Chim. Sin. 63 (2005) 269–273.
[22] A.G. Khaledi, S. Afshar, H.S. Jahromi, Mater. Chem. Phys. 135 (2012) 855–862.
[23] X.Y. Li, Z.R. Zhu, Q.D. Zhao, L.Z. Wang, J. Hazard. Mater. 186 (2011) 2089–2096.
[24] P.F. Chen, M.X. Du, H. Lei, Y. Wang, G.L. Zhang, F.B. Zhang, X.B. Fan, Catal. Commun. 18 (2012) 47–50.
[25] O.V. Manoilova, R. Olindoa, C.O. Areán, J.A. Lercher, Catal. Commun. 8 (2007) 865–870.
[26] J.R. Sohn, W.C. Park, Appl. Catal. A 239 (2003) 269–278.
[27] G.D. Yadav, B.A. Gawade, Catal. Today 207 (2013) 145–152.
[28] Z.R. Zhu, X.Y. Li, Q.D. Zhao, S.M. Liu, X.J. Hu, G.H. Chen, Mater. Lett. 65 (2011) 194–197.
[29] L.C. Peng, L. Lin, J.H. Zhang, J.B. Shi, S.J. Liu, Appl. Catal. A 397 (2011) 259–265.
[30] Q. Yu, X.J. Yao, H.L. Zhang, F. Gao, L. Dong, Appl. Catal. A 423–424 (2012) 42–51.
[31] C.Z. Liu, D.W. Meng, H.X. Pang, X.L. Wu, J. Xie, X.H. Yu, L. Chen, X.Y. Liu, J. Magn. Magn. Mater. 324 (2012) 3356–3360.
[32] O.B. Belskaya, I.G. Danilova, M.O. Kazakov, T.I. Gulyaeva, L.S. Kibis, A.I. Boronin, A.V. Lavrenov, V.A. Likholobov, Appl. Catal. A 387 (2010) 5–12.
[33] M.Y. Smirnova, A.V. Toktarev, A.B. Ayupov, G.V. Echevsky, Catal. Today 152 (2010) 17–23.
[34] M.L. Zhua, S. Li, Z.X. Li, X.M. Lu, S.J. Zhang, Chem. Eng. J. 185–186 (2012) 168–177.
[35] P.C. Wang, K. Yao, J. Zhu, X. Liu, T.T. Lu, M. Lu, Catal. Commun. 39 (2013) 90–95.